

# Influence of selective laser melting process parameters on the characteristics of SiC/Ti6Al4V(ELI) single tracks

Masenate Thamae<sup>1</sup>, Maina Maringa<sup>2</sup>, and Willie Du Preez<sup>3</sup>

<sup>1,2</sup>Department of Mechanical and Mechatronics Engineering, Central University of Technology, Free State. [masenate.a.thamae@gmail.com](mailto:masenate.a.thamae@gmail.com), [mmaringa@cut.ac.za](mailto:mmaringa@cut.ac.za)

<sup>3</sup>Centre for Rapid Prototyping and Manufacturing, Faculty of Engineering, Built Environment and Information Technology, Central University of Technology, Free State, [wdupreez@cut.ac.za](mailto:wdupreez@cut.ac.za)

**Abstract.** Process parameters of selective laser melting, such as track height, track width and depth of penetration, affect the characteristics of laser fused single tracks. The properties of additively manufactured 3D parts depend strongly on the quality of laser melted single tracks and resultant single layers. Layers formed with a good depth of laser penetration provide strong bonding between consecutive layers and the substrate. Poor depth of laser penetration leads to delamination of layers. In this study the effect of the critical process parameters of laser power, laser scanning speed, and laser linear energy density on the characteristics of SiC/Ti6Al4V(ELI) single tracks at different SiC volume fractions (5 %, 10 %, 15 %, 20 %, 25 % and 30%) was investigated. Phenomena, such as the keyhole effect, pre-balling, and balling of single tracks, were also investigated. The obtained results showed that increase of power at a constant speed increase both the track width and depth of penetration but the track height above the substrate is decreased.

## 1 Introduction

The titanium alloy, Ti6Al4V, is mostly used in engineering applications due to its excellent combination of high specific strength, good fatigue properties and outstanding corrosion resistance [1]. A limitation of titanium alloys is their poor abrasion resistance. This and other properties of these alloys may be improved by addition of Silicon Carbide (SiC) particles. These particles are used as reinforcement in the Ti6Al4V (ELI) matrix because of their excellent resistance to wear, sublimation temperature, specific stiffness, specific strength, hardness, and fracture toughness that are higher than those of a Ti6Al4V(ELI) matrix [2]. Silicon Carbide has a density of 3.21 g/cm<sup>3</sup> that is lower than that of Ti6Al4V(ELI) with a density of 4.45 g/cm<sup>3</sup>. Therefore, addition of SiC particles is expected

to reduce the density of SiC/Ti6Al4V (ELI) composites which should lead to fuel saving in automotive and aircraft applications [3]. The SiC particles have a coefficient of thermal expansion (CTE) of  $4.6 \times 10^{-6} /K$  that is lower than that of Ti6Al4V(ELI) ( $8.6 \times 10^{-6} /K$ ). Therefore, SiC/Ti6Al4V(ELI) composites should have CTEs that are closer to that of carbon fibre/epoxy resin composite to prevent buckling or separation at their interfaces in aircraft structures. Moreover, the resistance to wear of SiC particles that is higher than that of Ti6Al4V(ELI) will lead to SiC/Ti6Al4V(ELI) composites with higher wear resistance.

Sivakumaret et al. [3] investigated the mechanical properties of nano SiC particle reinforced Ti6Al4V matrix composites and reported that the inclusion of 5% SiC particles enhanced the compressive strength and hardness, and reduced the density. However, they observed that an increase of the content of SiC to 10% and 15% led to increased porosity that resulted in a decrease of the corresponding strength of the specimen. Seleso et al. [4] presented details on the design of a ceramic particulate composite to enhance the mechanical properties of Ti6Al4V. They reported that different mechanical properties were improved with an increase of the content of filler particles. Ramah et al. [4] found that with a maximum SiC volume fraction of 20 % in an aluminium matrix, cracking around the filler particles could be avoided. However, as the volume fraction increased above this value the hardness of the composite increased and initiation of cracks at the interfaces, which led to failure of the composites, increased.

Dash et al. [5] while investigating the behaviour of aluminium matrix composites under thermal stresses observed that ceramic reinforcements have large difference in CTE with the matrix which induce large residual stresses near the interfaces of the composites when they are cooled from fabrication temperatures. They then noted that the induced residual stresses at the interfaces affect the physical and mechanical properties of built parts. It is clear from the foregoing material that the overall behaviour of composites, including their response to heating as occurs in additive manufacturing, depend on the volume fraction of the reinforcement. This creates a need to carry out tests, and in the case of additive manufacturing build specimens, at different volume fractions of fillers to establish any volume fraction related trends that may exist.

In selective laser melting (SLM), three dimensional (3D) parts are formed by progressively building single tracks, multiple tracks, and layers fused onto each other, until the full part is built [6]. The properties of parts produced by this technology depend on the characteristics of each single track, the morphology of each layer and the cohesion of tracks and layers with each other [7]. Other factors that affect the properties of parts include the type of recoater used for spreading powder during the production of 3D parts and extraction of suspended electron particles from the build chamber in the Electron Beam Modelling (EBM) technology, which if not removed, would affect the produced parts. When the electrostatic forces exceed a critical value, the powder particles scatter or repel each other thus making the building process in EBM virtually impossible [8]. The formation of the molten pool and single track play a major role in the quality and mechanical properties of manufactured 3D objects.

When producing additively manufactured parts, continuous tracks are desirable because they lead to good bonding between adjacent tracks and result in minimal porosity of the final built parts [9]. Variation of process parameters of (laser power, scanning speed, layer thickness and hatch distance) leads to different track morphologies, such as pre-balling, balling, and the keyhole effect. High power with low scanning speed leads to a high energy

density that vaporizes the melt and causes deeper penetration, thus causing the keyhole effect. Yadroitsava et al. [10] investigated the formation of single tracks from Ti6Al4V at different laser power densities and found that at high laser power density, excessive input of energy led to the keyhole mode resulting in deep remelting of the substrate and formation of pores. The keyhole effect is undesirable in selective laser sintering because it leads to the formation of pores and irregular single tracks. According to the model of (Eagar et al., [11]), the cross section of the melt pool formed in the conduction mode is approximately semicircular. Thus, the melt pool depth is about half its width. Therefore, the keyhole effect with its deeper penetration causes the depth of the melt pool to be greater than half its width. Ideally, the melt pool penetration must be deep enough to achieve bonding with the previous layer, the width must be sufficient to merge with adjacent melt tracks and the depth-to-width ratio should be around 0.5 to avoid balling or the keyhole effect [12].

As the scanning speed increases at the same laser power, the melt pool temperature decreases, while surface tension and melt pool viscosity increase, thus leading to the formation of discontinuous tracks with irregular widths [7]. At higher scanning speeds, reduced energy input leads to lower depths of penetration that cause poor bonding between tracks and the first track and substrate. There are many parameters that affect the shape of the melt pool, the most common ones being Rayleigh instability and Marangoni convection. Marangoni convection is also known as surface tension driven convection, which is the convection along an interface between two fluids due to a surface tension gradient. Rayleigh instability is defined as the breaking up of liquid into droplets due to high surface tension and is a phenomenon that fully determines the pre balling and balling effects, which lead to the formation of irregular track widths [13].

Newby et al. [14]., studied the optimal process parameters for in-situ alloying of Ti6Al4V X%Cu and reported that at low effective power, the powder experienced lower temperatures, thus an increase of surface tension and viscosity leading to the formation of drops (balling). They further noted that the direction of fluid flow was determined by the Marangoni convection which is defined as the thermocapillary flow of fluid from areas of high surface tension to areas of low surface tension. A positive gradient was noted to cause the flow of fluid inwards, which led to the formation of keyholes and a negative gradient caused the flow of fluid outwards, thus resulting in the formation of shallow and wider melt pools, respectively.

In this paper the influence of selected critical SLM process parameters and volume fraction of SiC on the characteristics of SiC/Ti6Al4V(ELI) composites is investigated for the purpose of obtaining the best single tracks and for use in building multiple layers with good bonding and 3D parts with enhanced mechanical properties.

## 2 Methodology

Silicon carbide and Ti6Al4V(ELI) powders were mixed using a multi-tube rotary batch mixer where the constituent powders were loaded into six different containers in the mixer, mixed for a period of time, then discharged in individual batches. The multi-tube rotary batch mixer works on the principle of diffusion, which mechanism encourages the individual movement of particles within the vessel and does not require impellers to move them. Impellers lead to undesirable agglomerated and segregated powder mixtures. The SiC/Ti6Al4V(ELI) powder mixtures with SiC volume fractions varying from 5 % to 30 %, each volume fraction at a time, were deposited onto and levelled with a recoater blade on the build platform of an

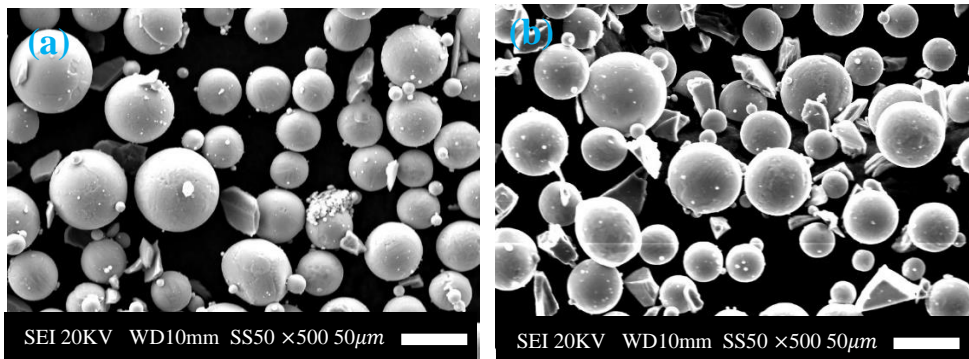
EOSINT M 280 machine with a layer thickness of 45  $\mu\text{m}$ , The EOSINT M 280 machine used is located at the Centre for Rapid Prototyping and Manufacturing (CRPM) of the Central University of Technology, Free State. A laser beam with a spot size of 80  $\mu\text{m}$  was then used to build single tracks. The single tracks were built on 50 mm  $\times$  50 mm Ti6Al4V plates. Laser powers of 100 W, 150 W, 200 W, 250 W, 300 W and 350 W were used with laser scanning speeds varying from 0.3 m/s to 2.5 m/s at each volume fraction of SiC. The laser beam diameter and powder layer thickness were kept constant.

Top surface analysis of the built tracks was done with A ZEISS Axio Scope.A1 Optical Microscope (OM) to identify track characteristics, such as pre-balling, balling, keyhole formation and continuity. After top surface analysis, the built plates were cut with a wire cutting machine to avail cross sections of the tracks. The cross sections were cut perpendicular to the track length, one cross-section per track. because the variation of the track widths along track lengths was observed to be continuous and did not conform to any pattern. Therefore, any statistical analysis of widths for several cross-sections was considered not to have any meaningful value and thus the choice of a single cross-section per track. The cut pieces were then mounted with a Struers Cito Press-1 machine. The mounting of pieces took 3.5 minutes and was done at a temperature and pressure of 180°C and 250 bar, respectively. The samples were subsequently cooled by water for 2 minutes. They were then polished, etched with Kroll's reagent, and thereafter analyzed using the ZEISS Axio Scope.A1 Optical Microscope. Finally, analysis of the polished cross-sectional areas was done to identify the geometrical characteristics of track height, width, and depth of penetration into the substrate.

### 3 Results and Discussion

#### 3.1 Homogeneity of SiC/Ti6Al4V(ELI) powder mixture

Homogenous powder mixtures were obtained at low volume fractions of 5 % and 10 %, while higher volume fractions of SiC particles led to an increase of agglomeration of both SiC and Ti6Al4V(ELI) particles. Figure 1 shows Scanning electron microscope images of SiC/Ti6Al4V (ELI) mixtures at different SiC volume fractions.



Clustering of  
Ti6AL4V(ELI) particles

Clustering of SiC  
particles

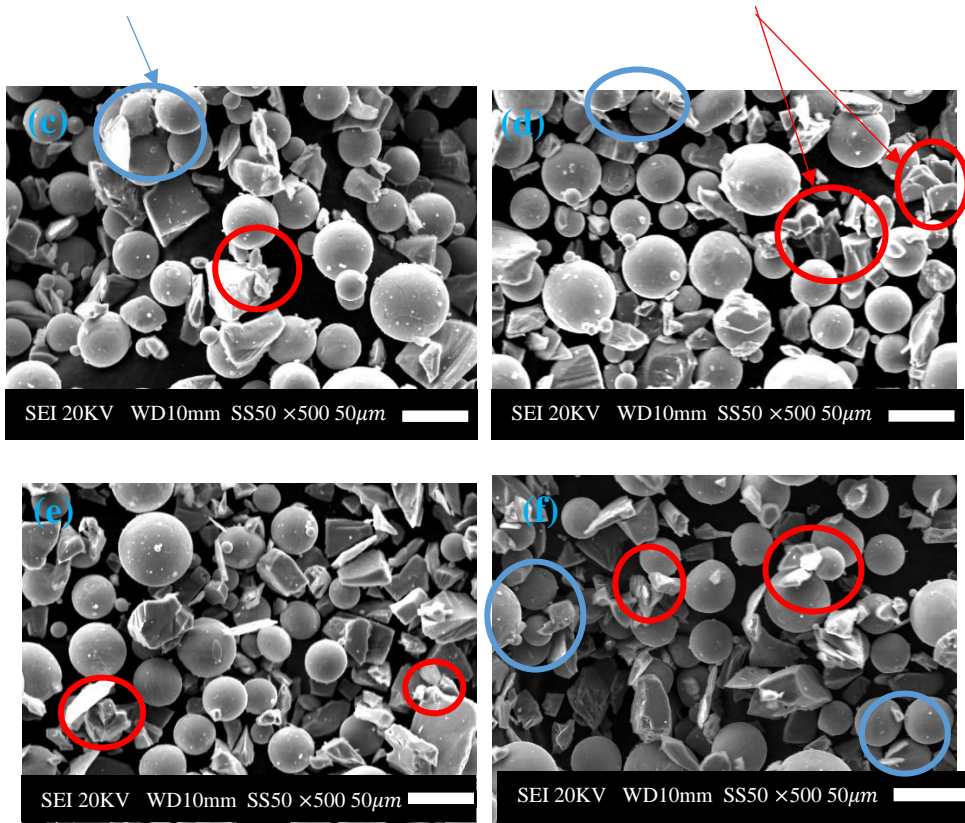


Figure1: SEM SE micrographs of SiC/Ti6Al4V (ELI) mixtures at different SiC volume fractions, at magnifications of 500 (a) 5 % SiC vol. fraction, (b) 10% SiC vol. fraction, (c) 15 % vol. fraction, (d) 20 % vol. fraction, (e) 25 % vol. fraction, and (f) 30 % vol. fraction indicating the clustering of particles.

Figure 1 shows that, for 5 % -10 % volume fractions the SiC particles are dispersed randomly among the Ti6Al4V (ELI) particles without clustering. Clustering of particles is seen to occur at a 15% SiC volume fraction and higher. The clustering of SiC particles are indicated by the red circles while that of Ti6Al4V particles are indicated by the blue circles in the micrographs presented in this work. This indicates a cut-off below which no agglomeration of particles occurs and vice versa. Therefore, this shows that agglomeration of these particles is dependent on the increase in loading of SiC particles.

### 3.2 The effects of laser scanning speed at a constant power of 200W

Increasing or decreasing the laser scanning speed at constant power is expected to reduce or increase the width of single tracks. This is for reasons that, as the laser scanning speed increases, the dwell time of the laser on the powder bed is reduced and so does the linear

energy density, which is equal to the ratio of laser power to scanning speed. This caused a decreasing trend in the width of the tracks, as shown in Figure 1.

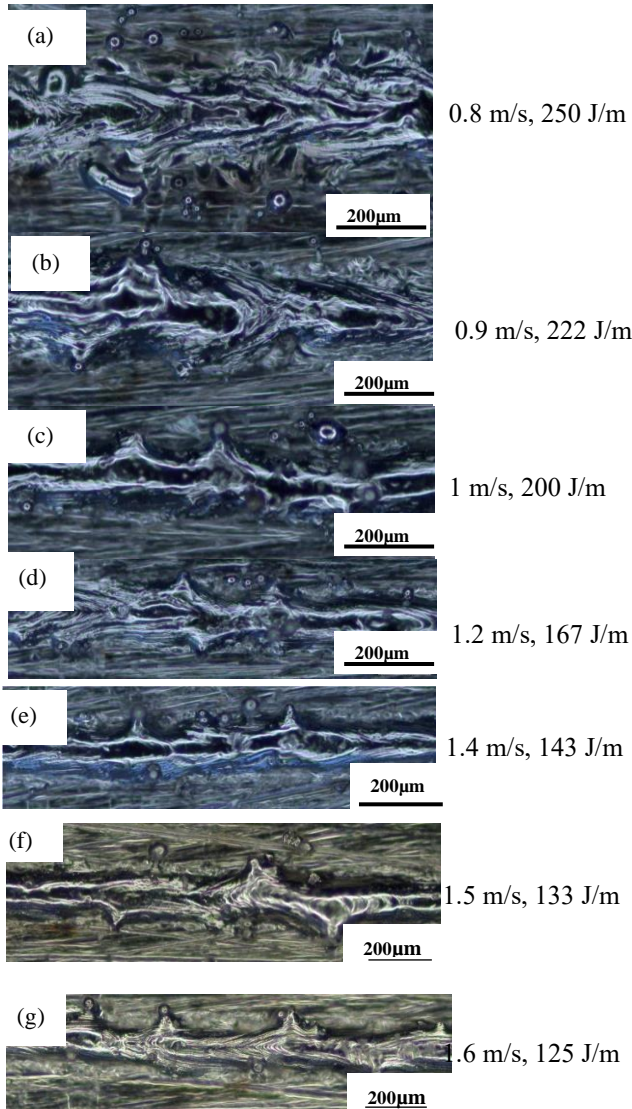


Figure 1: Single tracks produced at laser power of 200 W with varying scanning speeds from 0.8m/s to 1.6 m/s, resulting in linear energy densities ranging from 250 J/m to 125 J/m.

The widths of the tracks shown in Figure 1 reduced as the scanning speed increased. The widest tracks were produced for the tracks built at the lower speeds of 0.8 m/s and 0.9 m/s. This is thought to be a result of negative or low surface tension in the central regions of the melt pool, due to the reduction of surface tension and viscosity with increasing temperature, leading to radial outward flow of the molten pool metal and hence production of wider and shallower tracks [14], as shown in Figure 2 (a) and (b). Moreover, increased

scan speed while laser power was constant reduced the linear energy density, which also made the melt pool smaller due to less energy being deposited per unit length to melt the material. The geometrical characteristics of the cross sections through the tracks at laser power of 200 W with varying scanning speeds are shown in Figure 2.

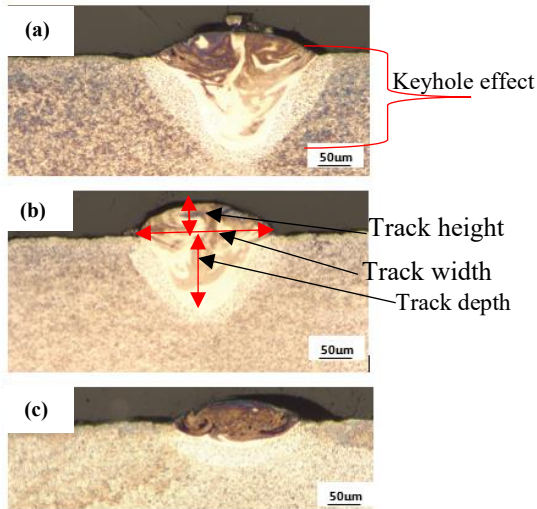


Figure 2: The cross-sectional images of the tracks produced at laser power of 200 W with scanning speeds of 0.8 m/s, 1 m/s and 1.6 m/s.

The single track shown in Figure 2(a) at the lowest scanning speed of 0.8 m/s and highest linear energy density of 250 J/m, indicates the keyhole effect. This is a result of excessive energy density, causing vaporization of the melt and a deeper penetration of the laser beam into the substrate [7]. The values of track width, depth of penetration and height above the substrate in this figure are 199 µm, 104 µm, and 31 µm, respectively, with a corresponding depth to width ratio of 0.5. A ratio greater than 0.5 leads to the formation of keyholes [11]. The keyhole effect negatively affects produced components because it leads to the formation of pores and irregular single tracks due to excessive energy density [9].

Further increase of the laser scanning speed to 1 m/s, reduced the energy density to 200 J/m which led to a decrease in the depth of penetration. Figure 2(b) shows an almost semicircular shape of the track cross-section, which is ideal for good metallurgical bonding with the substrate and with other previous layers. The width, depth, and width to depth ratio of this track were 162 µm, 70 µm, and 2.3, respectively. When the penetration depth is higher than the layer thickness, the previous layer will be remelted during laser sintering. This is the case here as the layer thickness ranges from 45 µm to 50 µm and the depth of penetration is 70 µm. Therefore, the previous layer or substrate will be remelted thus providing a good bond between the layers or present layer and the substrate (Guo et al. [16]). The lowest depth of penetration was observed in Figure 2(c), produced at the highest scanning speed of 1.6 m/s, which resulted in a reduction of the energy density and dwell time on the powder bed. Here the values of the track width, depth and depth to width ratio were 157 µm, 24 µm and 0.2, respectively. A ratio that is much less than 0.5 indicates poor depth of penetration into the substrate, as is the case in Figure 2(c).

### 3.3 The effects of constant linear energy density on single tracks

Figure 3 shows single tracks built at a constant linear energy density of 167 J/m, with scanning speeds varying from 0.6 m/s to 2.1 m/s and laser power ranging from 100 W to 350 W.

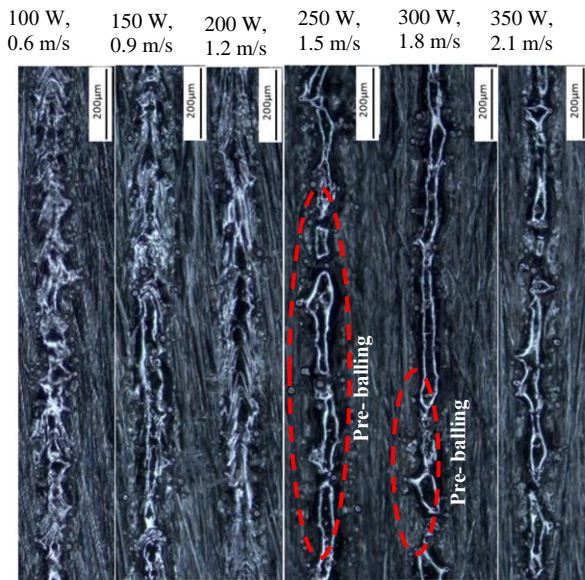


Figure 3: Single-track images at a constant linear energy density of 167 J/m, with varying scanning speeds and laser power.

Figure 3 shows that at the same linear energy density, the width of the single tracks reduced as the scanning speed and laser power increased. At low scanning speeds and power (0.6 m/s to 1.2 m/s and 100 W to 200 W) the tracks were almost continuous with constant widths. As the speed and power were increased to 1.5 m/s at 250 W and further to 2.1 m/s at 350 W, the track widths became narrower and discontinuous and exhibited the pre-balling effect. This can be explained by the fact that the faster the scanning speed, the less time there is for melting and fusion of powder. The narrow track widths may also be caused by the effect of increasing surface tension and Rayleigh instability with temperature. In such a case, fluid flows from the outer regions of track where the surface tension and viscosity are high to the areas of lower surface tension and viscosity towards the centre of the melt pool leading to the narrow track widths with deep penetration.

### 3.4 The effects of varying laser power at a constant scanning speed

The images of the single tracks at a constant laser scan speed of 0.8 m/s and varying values of laser power of 100 W, 150 W and 200 W are shown in Figure 4.

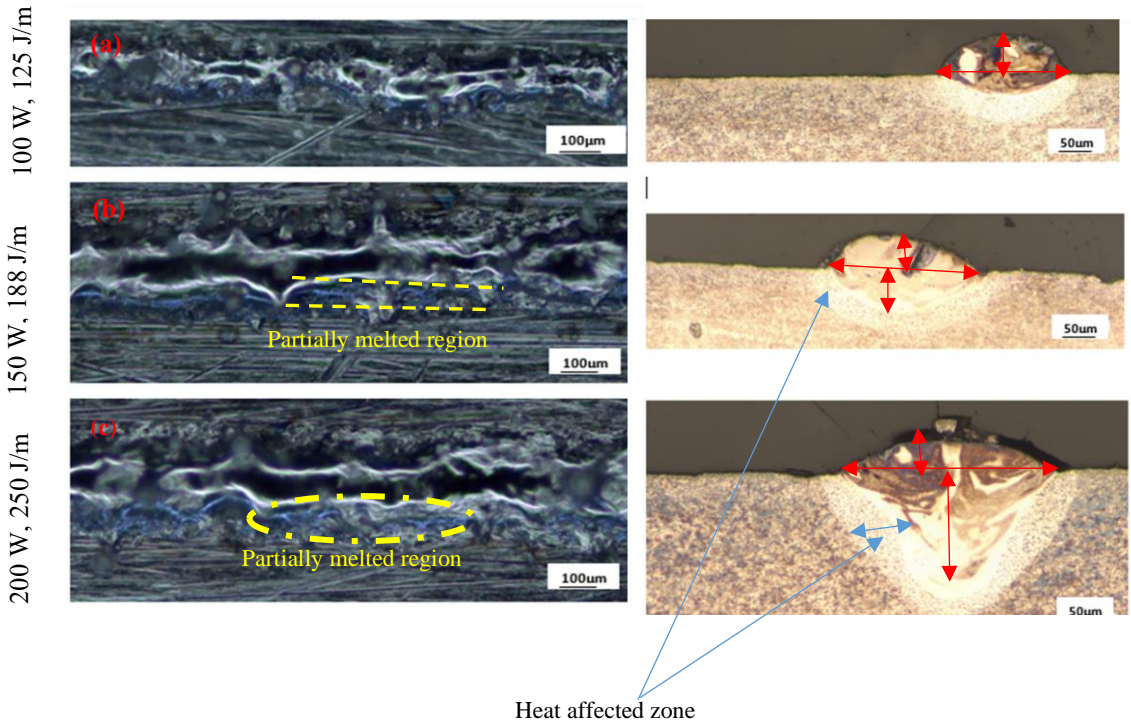


Figure 4: The top and cross-sectional views of tracks built at a constant scanning speed of 0.8 m/s and values of laser power varying from 100 W to 200 W.

The measured values of the geometric characteristics of track width, depth, and depth to width ratio of the printed tracks at a constant laser scanning speed of 0.8 m/s are shown in Table 1.

**Table 1:** Values of the track width, depth, height, and depth to width ratio produced at constant speed of 0.8 m/s

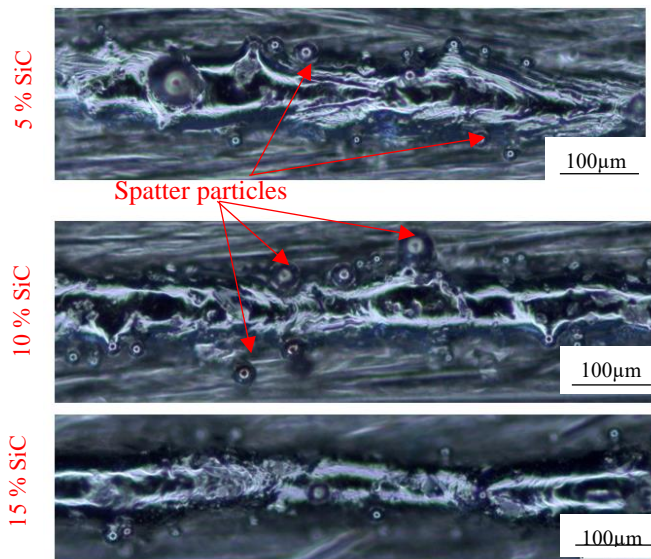
Process parameters	100 W, 125 J/m	150 W, 188 J/m	200 W, 250 J/m
<b>Geometrical characteristics</b>			
Height ( $\mu\text{m}$ )	36	34	30
Width ( $\mu\text{m}$ )	125	145	199
Depth ( $\mu\text{m}$ )	25	41	104
Depth to width ratio	0.25	0.3	0.5

It is clear from Table 1 that increasing the laser power at a constant laser scanning speed increased the linear energy density and thus the energy input. As is evident in Figure 4(a) and confirmed by the data in Table 1, the smallest depth of penetration, highest height above the substrate, lowest track width, and lowest depth to width ratio of 0.25 were observed at the lowest power of 100 W. Therefore, at this low power, the powder experienced lower temperatures and attendant high surface tension as well as viscosity, leading to drop formation (balling). As the laser power increased to 150 W, the depth of penetration and track width increased as seen in Table 1 but still with a depth to width ratio less than 0.5, which is indicative of poor penetration into the substrate. Further increase of the laser power to 200 W led to the formation of a wider track width with the best penetration depth to width ratio of 0.5.

A higher linear energy density corresponds to a higher energy input resulting in a higher temperature of the melt pool. Consequently, the particles near the track are heated through conduction or by the intense flow of the molten pool due to the higher prevailing temperature, thus widening the tracks and causing the particles at the edges of the track to melt partially [16]. This trend was observed on the top surface views of the tracks in Figure 4(b) and (c) that show partially melted regions indicated by yellow hatched lines increasing in size as the laser power increased. Kruth et al. [17], investigated the influence of the process parameters in selective laser melting and reported that laser power was the most significant process parameter determining the depth of penetration of the laser beam, while the scanning speed was a significant parameter in determining the width of the heat affected zone and the size of the melt pool. In this case the results shown in Figure 4 illustrate that laser power had an influence on the depth of penetration, track width and heat affected zone.

### 3.5 The effects of SiC volume fraction on the characteristics of single tracks

Here the effect of volume fraction of SiC on the characteristics of single tracks produced with constant laser power, scanning speed and linear energy density, is discussed.



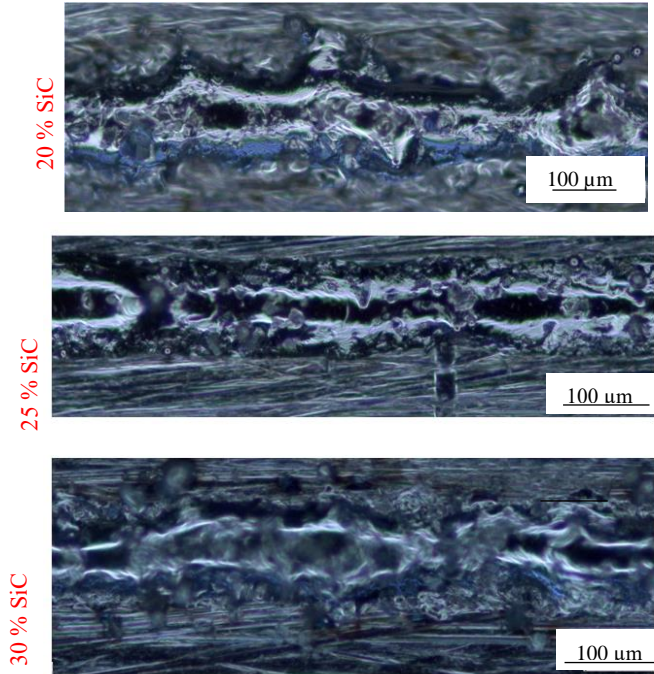


Figure 5: The top view of single tracks produced with a laser power of 200 W and scanning speed of 1.2 m/s at SiC volume fractions varying from 5% to 30%.

The tracks produced at 5 % to 15 % SiC volume fractions shown in Figure 5 exhibit a lot of spatter particles at the sides of the track that reduce in occurrence as the volume fraction of SiC increase from 20 % to 30%. At 5% SiC volume fraction, there is a large amount of spatter particles seen on top and on the sides of the track which is suggested to be the result of droplet spatter that occurs when low viscosity liquid is ejected from the molten pool due to induced Marangoni effect and recoil pressure. Track widths for 5 % to 15 % SiC volume fractions reduced due to smaller amounts of partially melted particles, however, the width of the tracks increased as the volume fraction of SiC was increased further from 20 % to 30 %. At a volume fraction of SiC of 30 %, a large region of partially melted particles occurred at the edges of the track due to increased conduction of heat. This is indicative of increased conductivity with increase of the SiC volume fraction.

The cross sections of single tracks shown in Figure 5 are presented in Figure 6 to further study the influence of SiC volume fraction on the width, heat affected zone (HAZ), depth, and the corresponding depth to width ratios.

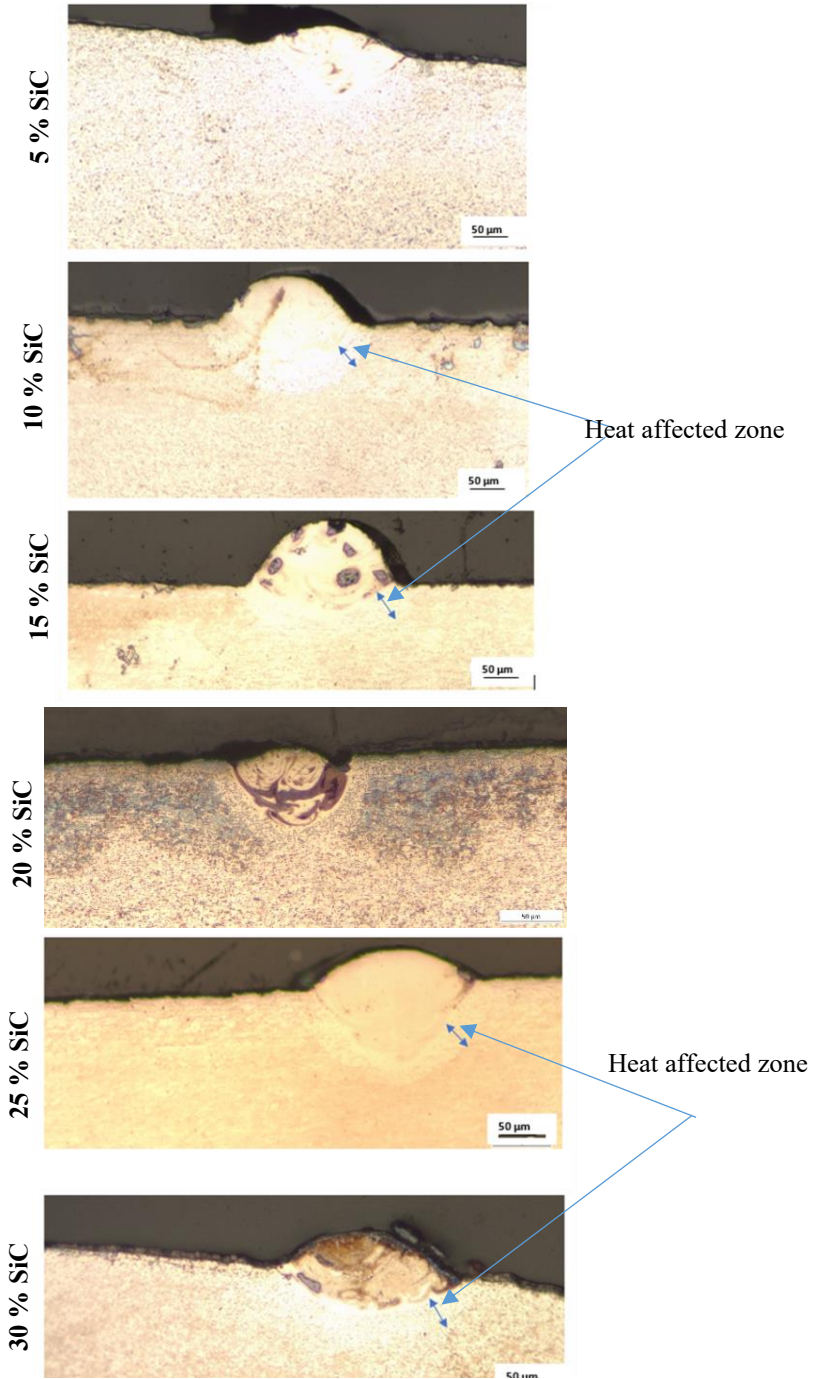


Figure 6: Cross sectional views of single tracks produced with a laser power of 200 W and scanning speed of 1.2 m/s at SiC volume fractions varying from 5% to 30%.

The width, and depth of penetration of the single tracks were measured from the cross sections shown in Figure 6 and are summarised in Table 2, together with their corresponding depth to width ratio.

**Table 2:** Values of width, depth, and depth to width ratio of single tracks produced at a laser power and speed of 200 W and 1.2 m/s.

	Geometrical characteristics	Width ( $\mu\text{m}$ )	Depth ( $\mu\text{m}$ )	Depth to width ratio ( $\mu\text{m}$ )
SiC volume fraction	5 % SiC	133	53	0.4
	10 % SiC	142	58	0.4
	15 % SiC	142	37	0.3
	20 % SiC	99	54	0.5
	25 % SiC	141	66	0.5
	30 % SiC	312	64	0.2

The heat affected zone is observed in Figure 6 to increase with increasing volume fraction of SiC from 10% SiC to 30% SiC. This is due to the higher heat conductivity of SiC particles that increases the overall thermal conductivity of the composite, also causing the particles at the edges of the tracks to be partially melted.

From the measured track values summarised in Table 2, depth of penetration is seen to decrease with increasing volume fraction from 5% to 15%. At 15 % volume fraction of SiC, the cross section shows poor penetration into the substrate and the formation of a hump above the substrate because of insufficient dwell time to form a continuous track. Further increase of the SiC volume fraction from 20 % to 25 % shows an increase in the depth of penetration followed by a decrease at a volume fraction 30%. Therefore, it can be concluded that the SiC volume fraction does not have a uniform effect on the depth of penetration. The same lack of a consistent variation with increasing volume fraction of SiC is observed with the width of tracks.

The optimum depth to width ratio of 0.5 was observed in Table 2 to prevail at the volume fractions of 20 % and 25 % both at an energy density of 167 J/m. At this ratio of 0.5 and energy density of 167 J/m, it was confirmed that the depth of penetration was sufficient to provide good bonding of multiple layers [7]. This implies that at these two volume fractions of SiC the process parameters used produced continuous and regular tracks with acceptable depth to width ratios. The same effect of SiC on the heat affected zone, as well as width and depth of single tracks observed at these process parameters, was observed for the process parameters of laser power, scan speed and energy density of 200 W, 1 m/s and 200 J/m. However, at a volume fraction of SiC of 20 %, the depth, height and width of the track dropped and later increased for SiC volume fractions of 25% and 30% SiC.

#### 4. CONCLUSIONS

- The study confirmed that a high energy input with a linear energy density of 250 J/m and a laser scanning speed of 0.8 m/s or a low energy input with a linear energy density of 125 J/m and scanning speed of 1.6 m/s at constant power of 200W gave rise to poor track characteristics.
- The study confirmed that increasing power from 100 W to 200W while keeping scanning speed of 0.8 m/s constant, increased the track width and depth of penetration while the height above the substrate was observed to decrease. However,

it was confirmed that increased depth of penetration due to high laser power of 200 W resulted in the formation of keyholes, while excessive linear energy density of 250 J/m resulted in unsuccessful formation of tracks and the occurrence of spatter particles.

- High SiC volume fractions from 20% to 30% were observed to have an increased effect on the increase of track width and heat affected zone, but a small influence on the depth of penetration.
- At volume fractions of 5 %,10 %, 15 % and 30 %, poor geometrical characteristics, such as irregular track widths, poor depth of penetration with depth to width ratios less than 0.5, were obtained. These are expected to lead to poor bonding of multiple tracks and layers and therefore poor mechanical properties of 3-D parts.
- The best volume fractions of SiC for the SiC/Ti6Al4V(ELI) built composites in this work were 20% and 25%.
- The response of the SiC/Ti6Al4V(ELI) composite to AM is dependent on volume fraction of the filler and so are the optimal process parameters.

### **Acknowledgements**

The financial support of the Department of Science and Innovation through the Collaborative Program in Additive Manufacturing is acknowledged for supporting this research.

## REFERENCES

1. G.Sivakumar, V.Ananthi, S.Ramanathan., Trans. Nonferrous Met. Soc. CHI, **27**,82-90 (2017).
2. J. C. Oh., E. Yun, M.G. Golkovski., S. Lee, Mater. Sci. and Eng.**351**, 88-108 (2003).
3. M. Seleso, M. Maringa and W. B. du Preez., Rapid Product Development Association of South African (RAPDASA) 21<sup>st</sup> Annual International Conference, Jappie van Lill Hall, Central University of Technology, free State, 3<sup>rd</sup> November 2020, South Africa, <https://site.rapdasa.org/pre-conference-seminar/.,41-55> (2020).
4. M.H. Rahman., H.M. Al Rashed, *Proc. Eng.*, **90**, 103-109(2014)
5. K.Dash., S.Sukumaran., B.C. Ray., *Sci. and Eng. Of Comp. Mater*, **23**, 1-20. (2016).
6. Y. Pupo, J. Delgado, L. Serenó, J. Ciurana., *P. Eng.* **63**, 370, (2013).
7. L. A Ramosena, B.S. Parker, T.C. Dzogbewu, W.B. du Preez, D.C. Blaine, *Proceedings of the 20th RAPDASA Annual International Conference*, 78-93. (2019).
8. A.Chiba., Y. Daino, K. Aoyagi., K. Yamanaka., K., 2021. *Mater.*, **14**, 4662. (2021).
9. S. Bertolli., A.J. Wolfer., M.J. Matthews, J.P.R. Delplanque, J.M. Schoenung., *Mat. Des.*, **113**, 331-340. (2017).
10. I. Yadroitsava, J.G. Els Booysen, I. Yadroitsev, SA. J. Ind. Eng, **26**, 86-95 (2015).
11. T.W. Eagar., N.S., Tsai, *Weld. J.*, **62**, 346-355, (1983).
12. T.M. Wischeropp, Effect of Laser Beam Profile on SLM Process. In *Advancement of Selective Laser Melting by Laser Beam Shaping*, 61-112, Springer Vieweg, Berlin, Heidelberg. (2021).
13. B. Fotovvati, S.F. Wayne, G. Lewis, E. Asadi, *Adv. Mater. Sci. and Eng.*, (2018).
14. E.B. Newby., I. Yadroitsava., D. Kouprianoff., *In-situ alloying of Ti6Al4V-x% CU structures by Direct Metal Laser Sintering*, Additive Manufacturing of Titanium Parts pre-conference seminar, 7 November 2017, Durban (2017).
15. K. Antony., N. Arivazhagan., *J.Eng. Sci. Tech.*, 10, 509-525
16. G.U.O. Yueling, J.I.A. Lina, K.O.N.G. Bin, W.A.N.G., Na, H. Zhang, *CHI. J. Aero.*, **31**,860-866., (2018).
17. J. Kruth. L. Thijs, F. Verrhaeghe, J. Craeghs. H. Van., *Acta Meter.* **58**, 3303-3312. (2010).